Synthesis and Properties of Metalloporphyrin Monolayers and Stacked Multilayers Bound to an Electrode via Site Specific Axial Ligation to a Self-Assembled Monolayer

David A. Offord, Sandra B. Sachs, Matthew S. Ennis, Todd A. Eberspacher, John H. Griffin,* Christopher E. D. Chidsey,* and James P. Collman*

Contribution from the Department of Chemistry, Stanford University, Stanford, California 94305

Received October 8, 1997

Abstract: A general method has been developed for the immobilization of metalloporphyrins at a gold electrode surface coated with a self-assembled monolayer (SAM). SAMs containing imidazole-terminated adsorbates are shown to bind a series of metalloporphyrins, including bis-acetonitrile octaethylporphyrinatoruthenium(II), Ru(OEP)(CH_3CN)$_2$; bis-acetonitrile octaethyltetraazaporphyrinato ruthenium(II), Ru(OETAP)(CH_3CN)$_2$; bis-acetonitrile tetra-(*p*-chlorophenyl)porphyrinatoruthenium(II), Ru(Tp-ClPP)(CH_3CN)$_2$; bis-acetonitrile octaethylporphyrinatoosmium(II), Os(OEP)(CH_3CN)$_2$; and carbonyl *meso*-tetramesitylporphyrinatoruthenium(II), Ru(TMP)(CO). The SAM/metalloporphyrin films have been characterized by optical ellipsometry, contact angle goniometry, X-ray photoelectron spectroscopy, grazing angle FT-IR spectroscopy, transmission visible spectroscopy, and electrochemistry. The results indicate that the metalloporphyrins are chemisorbed via axial ligand substitution of the metal center with the porphyrin ring parallel to the surface and the second axial ligand position normal to the surface. Scanning tunneling microscopy images of Ru(TMP)(CO) bound to the SAM corroborate this model. Axial ligation of metalloporphyrins to SAMs serves as the basis for an iterative, defined approach to the preparation of stacked single component and mixed metalloporphyrin multilayers on SAMs. In these materials, the bidentate ligand pyrazine serves as a bridge between successive metalloporphyrins in the stacks.

Introduction

The importance and versatility of the porphyrin macrocycle and its metalated complexes in nature have inspired considerable efforts to understand, mimic, and expand the role of metalloporphyrins through the use of model systems.[1] The rich redox chemistry of metalloporphyrins makes them ideal templates for the design of new electron-transfer catalysts. Attaching redox active metalloporphyrins to electrodes simplifies their electrochemical study and facilitates their use as catalysts in electrochemical cells.[2] Most work in this area has involved metalloporphyrins adsorbed on edge-plane graphite electrodes (EPGE).[3] Edge-plane graphite is a complex, heterogeneous surface containing many functional groups (quinones, phenols, carboxylic acids, etc.),[4] and it is believed that surface functionalities influence the redox properties of EGPE-bound metalloporphyrins through axial ligation.[5] Recently, iodine-modified Au(111)was used to anchor porphyrins directly to the gold surface.[6] Two clear advantages exist for the method presented in this work over either EPGE or iodine-modified Au electrodes: first, the role(s) played by surface functional groups in metalloporphyrin adsorption and in modulation of redox properties may be better understood through the use of defined electrodes which present a single type of axial ligand; second, if the attachment site density can be changed, the final concentration of the porphyrin on the surface will be controlled. Electrodes coated with self-assembled monolayers (SAMs) represent one such system, as the SAM end group functionality is easily controlled.[7] Due to their packing density and structural rigidity, SAMs separate an electrode from a redox active species via a thin hydrocarbon layer while still allowing for the passage of current between the two. This has previously been demonstrated by assembling alkyl mercaptans bearing covalently attached electroactive end groups (e.g., ferrocene[8] and ruthenium pentaamine[9]) on gold electrodes. Metalloporphyrins have been adsorbed to gold electrodes via alkyl mercaptan arms appended to the porphyrin ring.[10,11] Cobalt(II) porphyrins attached via this method were found to catalyze the reduction of O_2 to H_2O_2.[10b]

* To whom correspondence should be addressed.

(1) For a review, see: Collman, J. P.; Wagenknecht, P. S.; Hutchinson, J. E. *Angew. Chem., Int. Ed. Engl.* **1994**, *33*, 1537−1554.

(2) Murray, R. W. *Electroanalytical Chemistry: A Series of Advances*; Bard, A. J., Ed.; Marcel Dekker: New York, 1984; Vol. 13.

(3) (a) Schick, G. A.; Schreiman, I. C.; Wagner, R. W.; Lindsey, J. S.; Bocian, D. F. *J. Am. Chem. Soc.* **1989**, *111*, 1344−1350. (b) Wang, B.; Cao, X. *J. Electroanal. Chem.* **1991**, *309*, 147−158. (c) Ramachandraiah, G.; Bedioui, G.; Devynck, J. *J. Electroanal. Chem.* **1991**, *319*, 395−402. (d) Ngameni, E.; Laouénan, A.; L′Her, M.; Hinnen, C.; Hendricks, N.; Collman, J. P. *J. Electroanal. Chem.* **1991**, *301*, 207−226. (e) Collman, J. P.; Chng, L.; Tyvoll, D. *Inorg. Chem.* **1995**, *34*, 1311−1324.

(4) Ni, C. L.; Anson, F. C. *Inorg. Chem.* **1985**, *24*, 4754−4756. (b) Shi, C.; Anson, F. C. *Inorg. Chem.* **1990**, *29*, 4298−4305.

(5) Bettelheim, A.; Chan, R. J. H.; Kuwana, T. *J. Electroanal. Chem.* **1979**, *99*, 391−397.

(6) Kunitake, M.; Akiba, V.; Batina, N.; Itaya, K. *Langmuir* **1997**, *13*, 1607−1615.

(7) For reviews of SAMs, see: (a) Whitesides, G. M.; Laibinis, P. E. *Langmuir* **1990**, *6*, 87−96. (b) Ulman, A. *An Introduction to Ultrathin Organic Films from Langmuir Blodgett to Self-Assembly;* Academic Press: San Diego, 1991. (c) Dubois, L. H.; Nuzzo, R. G. *Annu. Rev. Phys. Chem.* **1992**, *43*, 437−463. (d) Ulman, A. *Characterization of Organic Thin Films: Materials Characterization Series−Surfaces, Interfaces, Thin Films;* Butterworth-Heinemann: Stoneham, MA, 1995.

S0002-7863(97)03528-2 CCC: $15.00
Published on Web 04/28/1998

In this paper, we describe general methods for the controlled preparation of defined metalloporphyrin monolayers and stacked multilayers on SAM-modified gold electrodes. The core feature of these methods is axial ligation of metalloporphyrins to imidazole groups present at the surface of a SAM. This provides a well-defined environment for analytical investigations, passivates the electrode surface, and allows for incremental variation in metalloporphyrin surface coverage. Relative to previous methods for attaching metalloporphyrins to gold electrodes, our approach is attractive in that it eliminates the need for chemical modification of the metalloporphyrin. We present the results of detailed surface analytical investigations of the monofacial metalloporphyrin acetonitrile octaethylporphyrinatoruthenium(II), (Ru(OEP)(CH_3CN)), ligated to imidazole-terminated, gold-supported SAMs. We demonstrate the generality of this approach to metalloporphyrin surface immobilization with a series of additional ruthenium and osmium porphyrin complexes. Finally, we show that axially ligated SAM/metalloporphyrin monolayers can serve as templates for the efficient, stepwise elaboration of pyrazine bridged, single component and mixed stacks of metalloporphyrins, which are of interest for their structural and physical properties.[12] This iterative approach to building multilayers could be implemented as a solid-phase synthesis of novel metalloporphyrin materials.[12g]

Experimental Section

General. Manipulations of oxygen- and water-sensitive compounds were performed in a nitrogen-filled Vacuum Atmospheres Co. drybox maintained at or below 2 ppm O_2. Oxygen levels were monitored with an AO 316-C trace oxygen analyzer.

Solvents. Ethanol (Gold Shield, 200 proof) was sparged with argon before use. Deionized/distilled water was used for all washings. Water purified by passage through a Milli-Q system was used for contact angle measurements. Methylene chloride used for routine rinsing of SAMs was obtained from Fisher and used as received. Solvents used for metalloporphyrin purification, metalloporphyrin deposition, and electrochemistry were distilled under argon from the following drying agents immediately prior to use: methylene chloride (phosphorus pentoxide), acetonitrile (calcium hydride), benzene and THF (sodium/benzophenone ketyl), methanol (magnesium turnings).

Adsorbates. *n*-Nonanethiol (Aldrich, 95%) and *n*-decanethiol (Aldrich, 96%) were purified by bulb-to-bulb distillation at ~0.075 Torr prior to use. 1-(10-mercaptodecyl)imidazole was prepared according to a literature procedure.[13] Final purification of this compound was carried out on a Perkin-Elmer LC200 HPLC equipped with a Rainin Dynamax 300A C18 preparatory column (25.4 cm × 21.4 mm i.d., 12-μm particle size) and a gradient of acetonitrile in water (with 0.1% trifluoroacetic acid, TFA). After an initial 5 min flow of 100% water at 5 mL/min, an acetonitrile gradient was introduced at a rate of 0.25%/min. The eluate was monitored at 207 nm, and the product eluted at 27% acetonitrile. The acetonitrile was removed under reduced pressure, and the remaining solution was extracted with three 100 mL portions of argon-sparged ethyl ether. The extracts were combined and washed with 100 mL of argon-sparged saturated aqueous sodium bicarbonate solution and three 100 mL portions of distilled water. To suppress disulfide formation, special care was taken to exclude oxygen during the isolation of the product. The ^{1}H NMR, ^{13}C NMR, and IR (KBr) spectra for the compound matched those reported.[13] Liquid secondary ion mass spectrum (LSIMS): MH^+ calcd *m*/*z* 241.2; found *m*/*z* 241.2.

Bis-acetonitrile Octaethylporphyrinatoruthenium(II), Ru(OEP)(CH_3CN)$_2$. Ru(OEP)(CH_3CN)$_2$ was synthesized by photolysis (mercury arc lamp) of Ru(OEP)(CO)(MeOH) (60 mg, 0.086 mmol) in acetonitrile (250 mL) under an argon purge following standard literature procedures.[14] The product was isolated in 65% yield (41 mg). UV−vis (toluene) λ_{max} 406 (Soret), 502, 528 nm. IR (KBr) 2259 cm^{-1} (ν_{CN}). ^{1}H NMR (C_6D_6) H_{meso} 9.98 (s, 4H); CH_2 4.02 (q, 7.6 Hz, 16H); CH_3 2.04 (t, 7.6 Hz, 24 H); CH_3CN −2.60 (s, 6H) ppm. LSIMS: M^+ (^{102}Ru) calcd *m*/*z* 716.3; found *m*/*z* 716.3.

Bis-acetonitrile Octaethyltetraazaporphyrinatoruthenium(II), Ru(OETAP)(CH_3CN)$_2$. Following a modified literature procedure,[14] a 20 mL glass photolysis well equipped with a Teflon vacuum valve was charged with Ru(OETAP)(CO)(CH_3OH) (15 mg, 0.022 mmol) and acetonitrile (12 mL). After two freeze/pump/thaw degassing cycles, the sample was photolyzed for 20 min and subjected to another freeze/pump/thaw cycle. The photolysis/freeze/pump/thaw procedure was repeated three times. The photolysis well was then taken into an inert atmosphere (N_2) glovebox where the solvent was removed in vacuo. The residue was purified by column chromatography on neutral alumina. Using a 1:1 mixture of acetonitrile and tetrahydrofuran, the product eluted as the major purple band. The solvent was removed in vacuo, and the resulting solid was dissolved in a minimal amount of acetonitrile. Upon drying, 14 mg (87% yield) of product was recovered. UV−vis (CH_2Cl_2) λ_{max} 560, 516, 540. IR (KBr) 2274 cm^{-1} (ν_{CN}). ^{1}H NMR (C_6D_6) CH_2 3.99 (q, 7.6 Hz, 16H); CH_3 2.10 (t, 7.6 Hz, 24 H); CH_3CN −2.53 (s, 6H) ppm. LSIMS: M^+ (^{102}Ru) calcd *m*/*z* 720.3; found *m*/*z* 720.2.

Bis-acetonitrile octaethylporphyrinatoosmium(II), Os(OEP)(CH_3CN)$_2$ was prepared from Os(OEP)(CO)(MeOH) using a procedure similar to that outlined for Ru(OETAP)(CH_3CN)$_2$. From 18 mg, 0.023 mmol, of starting material, 13 mg (70%) of the product was obtained. UV−vis (CH_2Cl_2) λ_{max} 388 (Soret), 486, 514. IR (KBr) 2237 cm^{-1} (ν_{CN}). ^{1}H NMR (C_6D_6) H_{meso} 9.30 (s, 4H); CH_2 3.91 (q, 7.5 Hz, 16H); CH_3 1.98 (t, 7.5 Hz, 24 H); CH_3CN −2.80 (s, 6H) ppm. LSIMS: M^+ (^{192}Os) calcd *m*/*z* 806.4; found *m*/*z* 806.3.

***meso*-Tetrakis(pentafluorophenyl)porphyrinatoruthenium(II), Ru(TPFPP).** The following procedure was adapted from the literature.[15,16] Ru(TPFPP)(CH_3CN)$_2$ (18 mg, 0.016 mM) was lyophilized from benzene

(8) (a) Chidsey, C. E. D.; Bertozzi, C. R.; Putvinski, T. M.; Mujsce, A. M. *J. Am. Chem. Soc.* **1990**, *112*, 4301−4306. (b) Creager, S. E.; Rowe, G. K. *Anal. Chim. Acta* **1991**, 246, 233−239. (c) Chidsey, C. E. D. *Science* **1991**, *251*, 919−922. (d) Collard, D. M.; Fox, M. A. *Langmuir* **1991**, *7*, 1192−1197. (e) Rowe, G. K.; Creager, S. E. *Langmuir* **1991**, *7*, 2307−2312. (f) De Long, H. C.; Donohue, J. J.; Buttry, D. A. *Langmuir*, **1991**, *7*, 2196−2202. (g) Groat, K. A.; Creager, S. E. *Langmuir* **1993**, *9*, 3668−3675. (h) Curtin, L. S.; Peck, S. R.; Tender, L. M.; Murray, R. W.; Rowe, G. K.; Creager, S. E. *Anal. Chem.* **1993**, *65*, 386-392. (i) Caldwell, W. B.; Chen, K.; Herr, B. R.; Mirkin, C. A.; Hulteen, J. C.; Van Duyne, R. P. *Langmuir* **1994**, *10*, 4109−4115. (j) Herr, B. R.; Mirkin, C. A. *J. Am. Chem. Soc.* **1994**, *116*, 1157−1158.

(9) Finklea, H. O.; Snider, D. A.; Fedyk, J. *Langmuir* **1990**, *6*, 371−378. (b) Finklea, H. O.; Hanshew, D. D. *J. Am. Chem. Soc.* **1992**, *114*, 3173−3181. (c) Finklea, H. O.; Hanshew, D. D. *J. Electroanal. Chem.* **1993**, *347*, 327−340. (d) Finklea, H. O.; Ravenscroft, M. S.; Snider, D. A. *Langmuir* **1993**, *9*, 223−227. (e) Redepenning, J.; Tunison, H. M.; Finklea, H. O. *Langmuir* **1993**, *9*, 1404−1407.

(10) (a) Zak, J.; Yuan, H.; Ho, K.; Woo, L. K.; Porter, M. D. *Langmuir* **1993**, *9*, 2772−2774. (b) Hutchison, J. E.; Postlethwaite, T. A.; Murray, R. W. *Langmuir* **1993**, *9*, 3277−3283. (c) Tyvoll, D. A., Ph.D. Thesis, Stanford University, Stanford, CA, 1995.

(11) Metalloporphyrins contained within enzymes have also been adsorbed onto gold-thiolate SAMs. Attachment has been achieved by electrostatic forces (Tarlov, M. J.; Bowden, E. F. *J. Am. Chem. Soc.* **1991**, *113*, 1847−1849) and by carbodiimide linkages through amino acid side chains (Collinson, M.; Bowden, E. F. *Langmuir* **1992**, *8*, 1247−1250).

(12) Hopfield, J. J.; Onuchic, J. N. Beratan, D. N. *Science* **1988**, *241*, 817−820. (b) Chen, J.; Seeman, N. C. *Nature* **1991**, *350*, 631−633. (c) Mathias, J. P.; Stoddart, J. F. *Chem. Soc. Rev.* **1992**, 215−225. (d) Kaszynski, P.; Friedli, A. C.; Michl, J. *J. Am. Chem. Soc.* **1992**, *114*, 601−620. (e) Wasielewski, M. R. *Chem Rev.* **1992**, 435−461 and references therein. (f) Segawa, H.; Kunimoto, K.; Susumu, K.; Taniguchi, M.; Shimidzu, T. *J. Am. Chem. Soc.* **1994**, *116*, 11193−11194. (g) Xiang, X.-D.; Sun, X.; Briceqo, G.; Lou, Y.; Wang, K.-A.; Chang, H.; Wallace-Freedman, W. G.; Chen, S.-W.; Schultz, P. G. *Science* **1995**, *268*, 1738−1740.

(13) Lee, T. R.; Carey, R. I.; Biebuyck, H. A.; Whitesides, G. M. *Langmuir* **1994**, *10*, 741−749.

(14) Anipas, A.; Buchler, J. W.; Gouterman, M.; Smith, P. D. *J. Am. Chem. Soc.* **1978**, *100*, 3015−3024.

(15) Camenzind, M. J.; James, B. R.; Dolphin, D., *J. Chem. Soc., Chem. Commun*. **1986**, 1137−1139.

(16) (a) Lindsey, J. S.; Wagner, R. W.; *J. Org. Chem*. **1989**, *54*, 828−836. (b) Chang, C. K.; Ebina, F. *J. Chem. Soc., Chem. Commun*. **1981**, 778−779.

(5 mL) and then pyrolyzed at 2×10^{-5} Torr and 230 °C for 5 h to yield Ru(TPFPP) (8 mg, 0.0075 mmol, 47%). ^{1}H NMR (C_6D_6) H_{meso} 8.01 (s, 8 H) ppm. UV−vis (toluene) λ_{max} 410 (Soret), 510, 530 nm.

Bis-dinitrogen *meso*-tetramesitylporphyrinatoruthenium(II), Ru(TMP)(N_2)$_2$ was prepared according to the literature procedure.[15] UV−vis (C_6H_6) λ_{max} 408 (Soret), 509, 525 nm. ^{1}H NMR (C_6D_6) H_β 8.82 (s, 8 H); mesityl H_m 7.20 (s, 8 H); mesityl CH_3 *p*-CH_3 2.49 (s, 12 H), *o*-CH_3 2.10 (s, 24 H) ppm.

Carbonyl *meso*-Tetramesitylporphyrinatoruthenium(II), Ru(TMP)(CO).[15] A sealed NMR tube containing Ru(TMP) (6 mg, 0.0068 mmol) and deuterated benzene (2.5 mL) was opened under a carbon monoxide atmosphere after a freeze/pump/thaw cycle. The dark brownish-red solution immediately turned a light orange-red. The excess carbon monoxide was removed by two freeze/pump/thaw cycles. The sample was taken into an inert (N_2) box where the solvent was removed in vacuo (6 mg, quantitative yield). UV−vis (CH_2Cl_2) λ_{max} 412 (Soret), 528. IR (CH_2Cl_2) 1942 cm^{-1} (ν_{CO}). ^{1}H NMR (C_6D_6) H_β 8.77 (s, 8H); mesityl H_m 7.19 (s, 4H); mesityl $H_{m'}$ 7.05 (s, 4H); mesityl CH_3 *p*-CH_3 2.43 (s, 12H), *o*-CH_3 2.15 (s, 12H), *o′*-CH_3 1.78 (s, 12H) ppm. LSIMS: M^+ (^{102}Ru) calcd *m*/*z* 910.3; found *m*/*z* 910.2.

Carbonyl Octaethylporphyrinatoosmium(II), Os(OEP)(CO). [Os(OEP)]$_2$ (7 mg, 0.0047 mmol) was quantitatively converted to Os(OEP)(CO) following a procedure described for the synthesis of Ru(TMP)(CO).[15] UV−vis (CH_2Cl_2) λ_{max} 390 (Soret), 508, 538 nm. IR (CH_2Cl_2) 1888 cm^{-1} (ν_{CO}). ^{1}H NMR (C_6D_6) H_{meso} 9.97 (s, 4 H); $-CH_2-$ 3.90 (m, 16 H); CH_3 1.88 (t, 24 H) ppm. LSIMS: M^+ (^{192}Os) calcd *m*/*z* 752.3; found *m*/*z* 752.3.

Bis-pyrazine octaethylporphyrinatoruthenium(II), Ru(OEP)(pyrazine)$_2$, was prepared according to the literature procedure.[17] UV−vis (toluene/pyrazine) λ_{max} 402 (Soret), 494, 520 nm. ^{1}H NMR (C_6D_6) H_{meso} 9.82 (s, 4 H); CH_2CH$_3$ 3.91 (m, 16 H); CH$_2$CH_3 3.88 (t, 24 H); $H_{(pyrazine)}$ 5.20 (d, 4 H); $H_{(pyrazine)}$ 1.79 (d, 4 H) ppm. LSIMS: M^+ (^{102}Ru) calcd *m*/*z* 794.3; found *m*/*z* 794.4.

Substrates. Polished silicon(100) wafers (2 in. diameter, Pure-Sil or 4 in. diameter, SiliconValley Microelectronics, Inc.) were cleaned by immersion in "piranha" solution (1:1 vol/vol 30% aqueous H_2O_2:H_2SO_4) at 20 °C for 10 min. (**WARNING**: Piranha solution reacts violently, even explosively, with organic materials.[18] It should not be stored or combined with significant quantities of organic material.) Clean substrates were rinsed thoroughly with deionized/distilled water, dried in a 2-propanol vapor bath, blown dry under a stream of argon, and transferred to an electron-beam vapor deposition chamber (5×10^{-7} Torr). Gold(111) substrates[19] were prepared by evaporating 10 nm of titanium followed by 100 nm of gold. Gold(111) substrates for STM study were prepared by electron-beam evaporation of 150 nm of gold (0.3 nm/s) onto freshly cleaved mica. The gold-coated mica was removed from the deposition chamber and annealed[20] in a quartz tube furnace at 480 °C for 24 h under a continuous flow of argon (scrubbed by hot titanium turnings).

Monolayer Formation. Mixed SAMs were formed in a nitrogen-filled inert atmosphere drybox by immersing freshly prepared gold substrates in solutions containing mixtures of mercaptans in oxygen-free ethanol or methanol (35 mL volume, 1 mM total mercaptan concentration). Each deposition solution was capped and stirred for 15 min before a freshly prepared gold substrate was introduced. The container was capped and stored at room temperature for 48 h, at which time the samples were removed from the drybox and rinsed successively with approximately 10 mL each of ethanol or methanol, methylene chloride, distilled water, and ethanol or methanol. Substrates were then blown dry under a stream of dinitrogen and characterized.

Porphyrin Deposition Procedure. In an inert atmosphere box, metalloporphyrins were deposited onto SAMs from a stirred 1 mM solution of metalloporphyrin in methylene chloride or benzene. The gold surfaces were removed from the porphyrin solution after 4 h, rinsed thoroughly, and allowed to dry in the box atmosphere prior to characterization.

Multilayer Deposition Procedure. This procedure is exemplified by the preparation of SAM/Ru(TMP)/pyrazine/Ru(TMP)(CO). In an inert (N_2) atmosphere box, Ru(TMP)(N_2) was deposited onto a mixed monolayer from a stirred 1 mM solution of Ru(TMP)(N_2)$_2$ in benzene. The gold surface was removed from the porphyrin solution after 15 min and rinsed thoroughly with benzene and allowed to dry in the box atmosphere. This surface was then placed in a stirred 1 mM solution of pyrazine in methylene chloride for 15 min and rinsed thoroughly with methylene chloride and benzene. This SAM/Ru(TMP)/pyrazine surface was once again placed in a stirred 1 mM solution of Ru(TMP)(N_2)$_2$ in benzene for 15 min and rinsed thoroughly with benzene. The resulting assembly was capped by placing the surface under an atmosphere of pure CO (15 psig) for 1 h.

Contact Angle Goniometry and Optical Ellipsometry. Measurement of contact angles and ellipsometric thicknesses are described elsewhere[21] and in the Supporting Information. A refractive index of 1.50 for the SAMs and SAM/metalloporphyrin films was assumed.[22]

X-ray Photoelectron Spectroscopy (XPS). X-ray photoelectron spectra were obtained on a Surface Science model 150 XPS spectrometer equipped with an Al Kα X-ray source, quartz monochromator, concentric hemispherical analyzer operating in constant analyzer mode, and a multichannel detector. The pressure in the analytical chamber during analysis was approximately 2×10^{-8} Torr. A takeoff angle of 35° from the surface was employed. Spectra of the C(1s) and Ru(3d) region (274−294 eV binding energy, 20 scans), the N(1s) region (388−408 eV binding energy, 70 scans), the Cl(2p1/2,2p3/2) region (191−211 eV binding energy, 20 scans), and the Au(4f) region (76−96 eV binding energy, 10 scans) were recorded with a 50 eV pass energy and a 150×800 μm spot size. The areas under the unsmoothed C(1s), Ru(3d), N(1s), Cl(2p1/2, 2p3/2), and Au(4f) peaks were measured (after a Shirley background subtraction) and corrected for the number of scans.

Grazing Angle FT-IR. Grazing angle (85° off surface normal) infrared spectra were obtained using p-polarized light on a Mattson RS 10000 FT-IR spectrometer. The spectra were taken in a dry air-filled sample compartment (water and carbon dioxide was removed by a Balston 74−5041 pure air generator). Five thousand scans were recorded at a resolution of 2 cm^{-1}. A narrow-band MCT detector, cooled with liquid nitrogen, was used to detect the reflected light. The moving mirror speed was 2.5 cm/s (40 kHz) in the forward (sampling) direction. The SAM spectra were ratioed to a background spectrum of a perdeuterated hexadecyl mercaptan SAM on gold.

Electrochemical Measurements. Surface electrochemical measurements were made in a cell formed by pressing a bored-out cone of poly(tetrafluoroethylene) against the monolayer. This defined the electrode area (0.43 cm^2).[8a] The electrolyte (0.2 M tetrabutylammonium hexafluorophosphate in methylene chloride), the counter electrode (platinum wire), and the reference electrode (Ag/Ag$^+$) were then placed in the bore. Solution electrochemistry was performed in a 3 mL conical vial with the same electrolyte, counter electrode, and reference electrode used in the surface electrochemistry, but employing a gold disk as the working electrode. Reference electrodes in both experiments were calibrated by measuring the ferrocene (Fc) redox potential which is known to be (+0.66V vs NHE)[23] in methylene chloride. All electrochemical measurements were made in an inert (N_2) atmosphere box

(17) Collman, J. P.; McDevitt, J. T.; Yee, G. T.; Leidner, C. R.; McCullough, L. G.; Little, W. A.; Torrance, J. B. *Proc. Natl. Acad. Sci. U.S.A.* **1986**, *83*, 4581−4585.

(18) (a) Dobbs, D. A.; Bergman, R. G.; Theopold, K. H. *Chem. Eng. News* **1990**, *17*, 2. (b) Wnuk, T. *Chem. Eng. News* **1990**, *26*, 2. (c) Matlow, S. L. *Chem. Eng. News* **1990**, *30*, 2.

(19) Polycrystalline gold substrates prepared by cold evaporative techniques have been shown to have extremely strong (>80%) Au(111) texture: (a) Chidsey, C. E. D.; Loiacono, D. N.; Sleator, T.; Nakahara, S. *Surf. Sci.* **1988**, *200*, 45−66. (b) Chidsey, C. E. D.; Loiacono, D. N. *Langmuir* **1990**, *6*, 682−691. (c) Nuzzo, R. G.; Fusco, F. A.; Allara, D. L. *J. Am. Chem. Soc.* **1987**, *109*, 2358−2368.

(20) DeRose, J. A.; Thundat, T.; Nagahara, L. A.; Lindsay, S. M. *Surf. Sci.* **1991**, *256*, 102−108.

(21) Offord, D. A.; John, C. M.; Griffin, J. H. *Langmuir* **1994**, *10*, 761−766.

(22) Swalen, J. D.; Santo, R.; Take, M.; Fischer, J. *IBM J. Res. Dev.* **1977**, *21*, 169−175. The refractive index of metalloporphyrins on the SAM is unknown. Therefore, the observed thickness increases are qualitative rather than quantitative measurements.

(23) Astruc, Didier. *Electron Transfer and Radical Processes in Transition-Metal Chemistry*; VCH Publishers: New York, 1995; p 144.

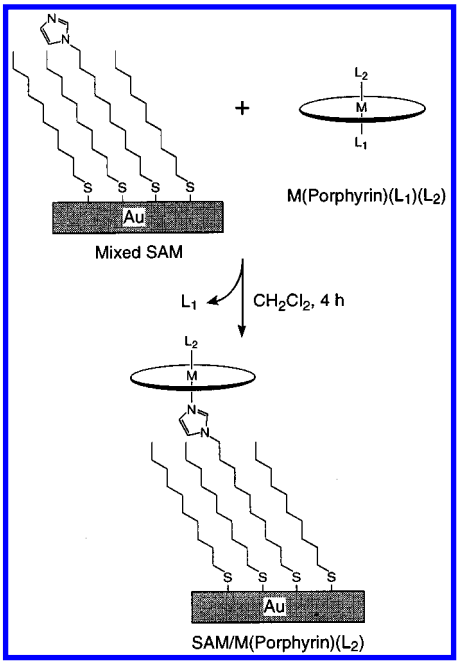

Figure 1. Deposition procedure and proposed mode of attachment of M(porphyrin)(L_2) to a mixed SAM of C9-SH and imid-SH on a planar gold substrate. L_1 is the more labile ligand.

with a PAR 273 potentiostat interfaced to a personal computer. The PAR 273 was modified to provide an input potential that was a smooth ramp in time.

Scanning Tunneling Electron Microscopy. Images were obtained in air on a Nanoscope-III instrument (Digital Instruments) equipped with a Pt/Ir wire tip sharpened by mechanical cutting. All images were obtained in height mode (constant current) and low-pass filtered. The *x* and *y* distances of the piezo scanner were calibrated with a pyrolytic graphite surface. The *z* distance was calibrated to the atomic steps on annealed gold substrates. Voltages and currents for individual images are given in the figure heading. To avoid destructive imaging, very large tunneling impedances were employed. Generally, sample-to-tip resistances were in the range of 0.6 and 33 GΩ.

Results

I. Axially Ligated Metalloporphyrin Monolayers. Approach. In the approach to metalloporphyrin surface immobilization presented here, a specific end group of a previously formed SAM serves as the axial ligand for the metal complex (Figure 1). An imidazole was chosen as the end group for these studies due to its high affinity for the metalloporphyrins of interest and its lack of competitive chemistry. An imidazole-terminated SAM is formed by immersing a gold surface in a solution containing a long-chain adsorbate bearing mercaptan and imidazole terminal groups. The SAM is then immersed in a solution of a metalloporphyrin bearing weakly bound or no axial ligands. The metalloporphyrin is immobilized by axial ligation to the SAM. The hydrocarbon backbone of the SAM holds the complex at a defined distance from the electrode and passivates the electrode surface.

Self-Assembled Mixed Monolayers (SAMs) and Self-Assembled Mixed Monolayers with Bound Ru(OEP)-(CH_3CN)−SAM/Ru(OEP)(CH_3CN). A series of mixed SAMs formed from the combination of *n*-nonanethiol (C9-SH) and 1-(10-mercaptodecyl)imidazole (imid-SH) were prepared and characterized. Monolayers were deposited by immersing freshly prepared gold(111)-coated silicon wafers in ethanol or methanol solutions of the adsorbates (1 mM total concentration) for 2 days at room temperature. The solution mole fraction of Imid-SH (χ_{soln} = [Imid-SH]/([Imid-SH] + [C9-SH])) was varied from 0 to 1 in order to produce monolayers with a range of surface compositions (χ_{SAM} = [Imid-S-Au]/([Imid-S-Au] + [C_9-S-Au])). The resulting series of mixed SAMs was then immersed in a 1 mM solution of Ru(OEP)(CH_3CN)$_2$ in methylene chloride under a dinitrogen atmosphere for 4 h[24] at room temperature to yield the SAM/Ru(OEP)(CH_3CN) series. Monolayers were characterized by X-ray photoelectron spectroscopy (XPS), optical ellipsometry, contact angle goniometry, grazing angle FT-IR spectroscopy, electrochemistry, transmission visible spectroscopy,[25] and scanning tunneling microscopy (STM).

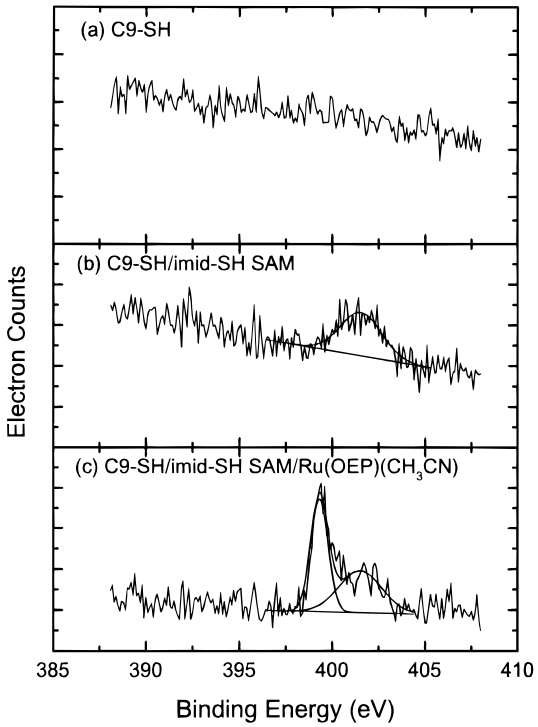

Figure 2. Comparison of the XPS N_{1s} between several monolayers made on Au(111). (a) A C9-SH monolayer after immersing in 1 mM Ru(OEP)(CH_3CN)$_2$ for 4 h. (b) A mixed monolayer of C9-SH and imid-SH formed where $\chi_{soln} = 0.5$. (c) The same monolayer described in (b) after immersing in 1 mM Ru(OEP)(CH_3CN)$_2$ for 4 h.

Due to the large van der Waals area of the porphyrin macrocycle (200 Å^2)[26] relative to that of alkyl mercaptan adsorbates (21.4 Å^2),[27] it is expected that only a fraction of the imidazoles in a $\chi_{soln} = 1.0$ SAM could ligate a metalloporphyrin as indicated in Figure 1. If the imidazole-terminated adsorbates were perfectly distributed, maximum metalloporphyrin coverage would be reached at $\chi_{SAM} = 0.11$.

XPS. The nonanethiol (C9-SH) and 1-(10-mercaptodecyl)-imidazole (imid-SH) SAMs and the imid-SH SAM/Ru(OEP)-(CH_3CN) and SAM/Ru(Tp-ClPP)(CH_3CN) series were characterized by XPS. We used this technique to determine the surface atomic compositions which show the presence or absence of certain species in the monolayer under various deposition conditions. Figure 2 compares the N(1s) regions of the XPS spectra of three different monolayers: C9-SH SAM submersed in Ru(OEP)(CH_3CN) for 4 h, C9-SH/imid-SH mixed monolayer, and C9-SH/imid-SH monolayer submersed in Ru(OEP)(CH_3CN) for 4 h. Each of the three monolayers were treated with the

(24) Longer deposition times (up to 24 h) resulted in no noticeable increase in the amount of adsorbed metalloporphyrin.

(25) These data are presented in the Supporting Information.

(26) Collman, J. P.; Eberspacher, T. A., unpublished crystallographic data.

(27) Strong, L.; Whitesides, G. M. *Langmuir* **1988**, *4*, 546−558.

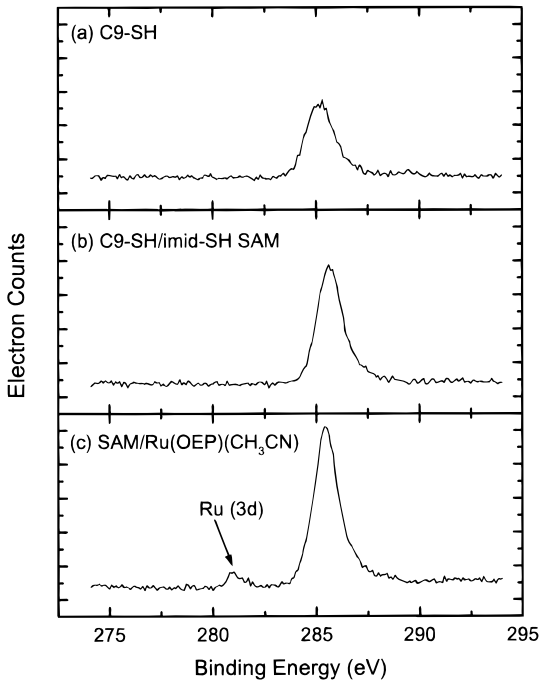

Figure 3. Comparison of the XPS C_{1s} region between several monolayers made on Au(111). (a) A C9-SH monolayer after immersing in 1 mM $Ru(OEP)(CH_3CN)_2$ for 4 h. (b) A mixed monolayer of C9-SH and imid-SH formed where $\chi_{soln} = 0.5$. (c) The same monolayer described in (b) after immersing in 1 mM $Ru(OEP)(CH_3CN)_2$ for 4 h.

same rinse procedure. In Figure 2a, one notes the distinct absence of nitrogen signal for the C9 monolayer, as expected, since there is no ligand anchor present to dock the porphyrin, the only nitrogen-containing species present in this experiment. Figure 2b shows that the imidazole nitrogens in the monolayer matrix yield a signal indicative of the presence of only one species of nitrogen. In Figure 2c, the nitrogen signal is partitioned into two discernible peaks: the sharper peak at lower binding energy is assigned as the porphyrin nitrogens while the broader peak at higher binding energy corresponds to the imidazole nitrogens as seen in panel b. One can conclude *qualitatively* that there is less than one porphyrin for every imidazole present in the monolayer because the integrals of the peaks in Figure 2c are roughly the same. If there were a metalloporphyrin for every imidazole, the number of nitrogens represented in the integral would be four to two. However, that analysis does not take into account attenuation factors for the imidazole nitrogens which are buried under the porphyrin. Any correction of this type would only strengthen the qualitative argument. We conclude that the porphyrin coverage is not limited by a shortage of ligand sites.

Figure 3 shows the carbon region for the same set of monolayers described above. In Figure 3a, the carbon signal for a C9-SH monolayer is shown. The second plot, Figure 3b, shows a relative increase of the carbon signal to that shown in Figure 3a when a mixed monolayer of C9-SH/imid-SH is present—more carbons are in the monolayer; therefore an increase is expected. An imid-SH/$Ru(OEP)(CH_3CN)$ monolayer is shown in Figure 3c. The signature feature in this panel is the presence of a distinct peak at lower binding energy than the carbon. This peak is assigned to Ru(3d) whose only origin can be from the porphyrin. The nitrogen and carbon XPS data show that the porphyrin only attaches to the monolayer surface when there is a site present to which it can bind. XPS data for another porphyrin, $Ru(Tp\text{-}ClPP)(CO)(CH_3CN)$ in a KBr matrix

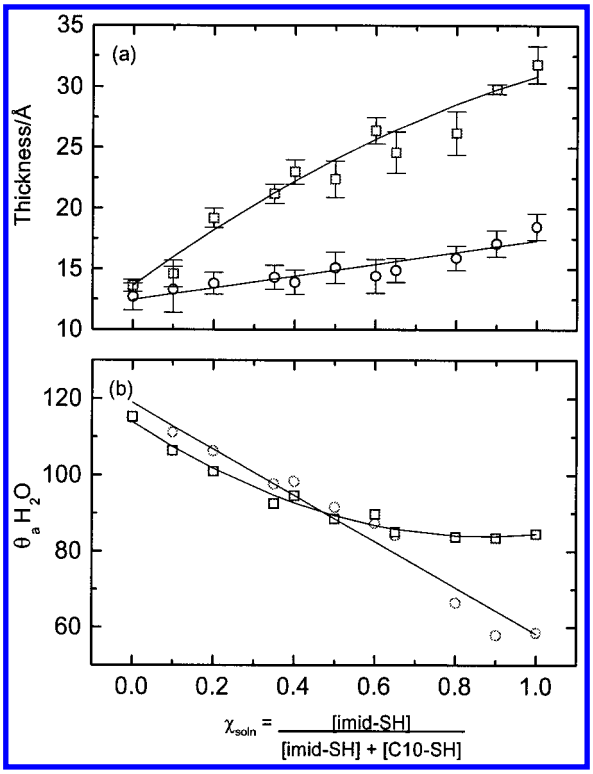

Figure 4. Ellipsometric thickness and contact angle goniometry data as a function of χ_{soln} for mixed monolayers of C9-SH and imid-SH before (circles) and after (squares) immersing in 1 mM $Ru(OEP)(CH_3CN)_2$ for 4 h: (a) ellipsometric thickness; (b) advancing water contact angles ($\theta_a(H_2O)$). Curves are provided as guides to the eye.

and on an imidazole-containing monolayer, can be found in the Supporting Information.

Ellipsometry. A series of SAMs and the resulting SAM/$Ru(OEP)(CH_3CN)$ films were characterized by optical ellipsometry to determine film thickness (Figure 4a). Thicknesses for the SAMs increased from 13 to 19 Å as χ_{soln} was increased from 0 to 1. The thickness of the SAM/$Ru(OEP)(CH_3CN)$ films increased from 14 to 32 Å over the same range of χ_{soln}. The ellipsometric thickness values at $\chi_{soln} = 0$ for the SAM, and the SAM/$Ru(OEP)(CH_3CN)$ films were the same within experimental precision (±2 Å). Thicknesses of the SAM series that had been exposed to $Ru(OEP)(CH_3CN)_2$ increased at a greater rate than the SAM series until a maximum difference ($\Delta d = 13$ Å) was reached with the $\chi_{soln} = 1$ surface.

Contact Angle Goniometry. The SAM series and the resulting SAM/$Ru(OEP)(CH_3CN)$ series were characterized by water contact angle goniometry to determine wettability. The observed contact angles are plotted as a function of χ_{soln} in Figure 4b. SAM advancing water contact angles decreased with χ_{soln} from 115° ($\chi_{soln} = 0$) to 59° ($\chi_{soln} = 1$). Following immersion of the SAMs in the $Ru(OEP)(CH_3CN)_2$ solution, the contact angles initially decreased with χ_{soln} but approached a limiting value of 85° near $\chi_{soln} = 0.50$. Thus, SAM/$Ru(OEP)(CH_3CN)$ surfaces reach limiting wetting properties at moderate surface concentrations of imidazole groups. This behavior indicates that the surface is covered with metalloporphyrins near $\chi_{soln} = 0.50$; therefore $\chi_{soln} = 0.5$ was used for monolayer formation in all XPS and electrochemical studies.

Electrochemistry. Figure 5a presents the cyclic voltammogram (CV) of $Ru(OEP)(CH_3CN)_2$ in solution as well as the CV of the blank electrolyte. Figure 5b shows $Ru(OEP)(CH_3CN)$ after attachment to a C9-SH/imid-SH monolayer along with two control experiments: a C9-SH/imid-SH monolayer without

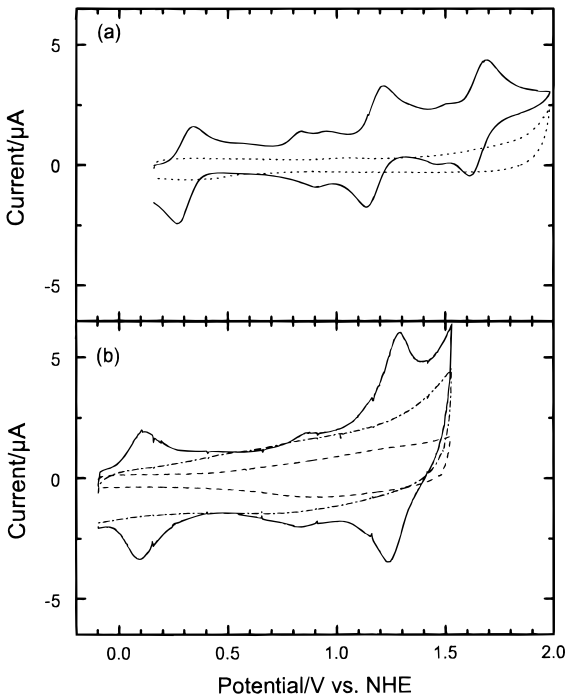

Figure 5. CVs showing redox couples of (a) solid line, Ru(OEP)-$(CH_3CN)_2$ in 0.2 M tetrabutylammonium hexafluorophosphate/methylene chloride solution; dotted line, 0.2 M tetrabutylammonium hexafluorophosphate in methylene chloride; (b) solid line, a $\chi_{soln} = 0.5$ SAM/Ru(OEP)(CH_3CN); dotted line, C9-SH soaked in Ru(OEP)-$(CH_3CN)_2$ for 4 h and rinsed as per the procedure described; dot−dashed line, SAM ($\chi_{soln} = 0.5$) without porphyrin soak. The scan rate in all cases was 100 mV/s.

porphyrin and a C9-SH monolayer soaked in Ru(OEP)(CH_3-$CN)_2$. The solution electrochemistry (Figure 5a) shows three reversible redox couples of Ru(OEP)$(CH_3CN)_2$ with peaks at 0.304, 1.174, and 1.650 V vs NHE as well as an irreversible set straddling 0.9 V vs NHE.[28] The first oxidation peak at 0.304 V is known to be the $Ru^{III/II}$ couple,[29] while the second and third peaks are most likely the $Ru^{IV/III}$ and porphyrin-centered oxidations;[29−31] however, the electrochemical assignment of peaks to particular chemical species is unresolved.[30,31] When Ru(OEP)(CH_3CN) is attached to the SAM surface, we assign the $Ru^{III/II}$ peak to be at 0.103 V vs NHE (Figure 5b) and the second peak at 1.263 V vs NHE to be either the $Ru^{IV/III}$ or a porphyrin-centered oxidation. The surface-bound porphyrin CV has symmetric peaks reflecting the fact that the redox species no longer have to diffuse to the electrode; it also shows that the electron transfer is kinetically fast on the time scale of the experiment, otherwise the oxidation and reduction waves would occur at different potentials. Ten CV scans caused no noticeable loss of peak area over the potential range in Figure 5b, indicating reasonable stability of the monolayer. The C9-SH/imid-SH monolayer CV has a larger background current than the unfunctionalized C9-SH SAM presumably because the imidazoles in the mixed monolayer do not pack as well as a pure C9-SH SAM. This allows electrolyte ions to approach closer to the electrode and produce a larger charging current.[19b]

From the surface-bound Ru(OEP)(CH_3CN) CV in Figure 5b, we can quantify the porphyrin coverage on the monolayer.

(28) These extraneous peaks are attributable to a small amount of impurity in the porphyrin and, in our hands, are always observed.

(29) Brown, G. M.; Hopf, F. R.; Ferguson, J. A.; Meyer, T. J.; Whitten, D. G. *J. Am. Chem. Soc.* **1973**, *95*, 5939−5942.

(30) Kadish, K. M. *Progress in Inorganic Chemistry;* Lippard, S. J., Ed.; John Wiley & Sons: New York, 1986; pp 437−460, 549−559.

(31) Bond, A. M.; Khalifa, M. *Aust. J. Chem.* **1988**, *41*, 1389−1406.

Table 1. Advancing Water Contact Angles and Ellipsometric Thicknesses of Ru(OEP)(CH_3CN), Ru(OETAP)(CH_3CN), Os(OEP)(CH_3CN), and Ru(TMP)(CO) Metalloporphyrins Bound to a Monolayer ($\chi_{soln} = 0.75$) Compared to the Corresponding SAM without Metalloporphyrin

surface	$\theta_a(H_2O)$	thickness (Å)
SAM	79	15
SAM/Ru(OEP)(CH_3CN)	88	25
SAM/Ru(OETAP)(CH_3CN)	89	28
SAM/Os(OEP)(CH_3CN)	90	24
SAM/Ru(TMP)(CO)	93	25

Integration of the first set of redox peaks at 0.103 V and normalization by the scan rate and electrode area gives an average charge density of 5.3×10^{-6} C/cm^2. Using the same procedure on the second set of peaks[32] at 1.263 V yields an average charge density of 5.7×10^{-6} C/cm^2. Dividing the average of these values by the charge on an electron, an effective area of 291 Å^2 per Ru(OEP)(CH_3CN) is calculated. As described in the Supporting Information, one physical interpretation of the electrochemical data comes from a proposed packing model involving a $\sqrt{13}x\sqrt{13}R13.9°$ superlattice which allows commensurate packing of porphyrins 200 Å^2 in size on the $\sqrt{13}x\sqrt{13}R30°$ lattice. The model gives an effective area of 281 Å^2 per porphyrin, in good agreement with our experimental result, suggesting that our electrochemical coverage is indeed reasonable.

Chemisorption versus Physisorption of Metalloporphyrins at the SAM Surface. Experiments were carried out to determine whether specific ligation to the imidazole terminus of the SAM was critical for metalloporphyrin binding. First, attempts to deposit Ru(OEP)$(CH_3CN)_2$ from methylene chloride solution in the presence of 1 mM trifluoroacetic acid were unsuccessful. The metalloporphyrin was determined to be unaffected by the dilute acid through ^{1}H NMR and UV−vis analysis. Characterization of the protonated SAM revealed that the dilute acid did not disrupt the monolayer but did reduce the advancing water contact angle as expected if the imidazole termini were protonated. Second, attempts to deposit Ru(OEP)-(1,5-dicyclohexylimidazole)$_2$, in which the axial ligands are much less labile than those of Ru(OEP)$(CH_3CN)_2$, were unsuccessful. Finally, the XPS results and electrochemistry data for C9-SH monolayers treated with porphyrin that were discussed previously bolster the argument that physisorption onto methyl-terminated monolayers is not taking place, implying that it is chemisorption that occurs when adsorbed porphyrin is observed.

Other Metalloporphyrins. Following the procedure described for preparation of SAM/Ru(OEP)(CH_3CN), bis-acetonitrile octaethyltetraazaporphyrinatoruthenium(II) Ru(OETAP)-$(CH_3CN)_2$, bis-acetonitrile octaethylporphyrinatoosmium(II) Os(OEP)$(CH_3CN)_2$, and carbonyl *meso*-tetramesitylporphyrinatoruthenium(II) Ru(TMP)(CO) were adsorbed on $\chi_{soln} = 0.75$ SAMs. The advancing water contact angles and ellipsometric thicknesses for these surfaces and SAM/Ru(OEP)(CH_3CN) are summarized in Table 1. The advancing water contact angles and thicknesses for the various SAM/metalloporphyrins are similar, indicating that the metalloporphyrins form similar structures on the SAM.

SAM/Ru(OETAP)(CH_3CN) (0.58 V, 1.21 V vs NHE) and SAM/Os(OEP)(CH_3CN) (0.59 V, 1.25 V vs NHE) each

(32) Not knowing the specific identity of this species does not hinder the analysis here. Since we have a 1-electron oxidation of either $Ru^{IV/III}$ or the porphyrin which are present in a 1:1 stoichiometry, the CV area still leads to a porphyrin coverage.

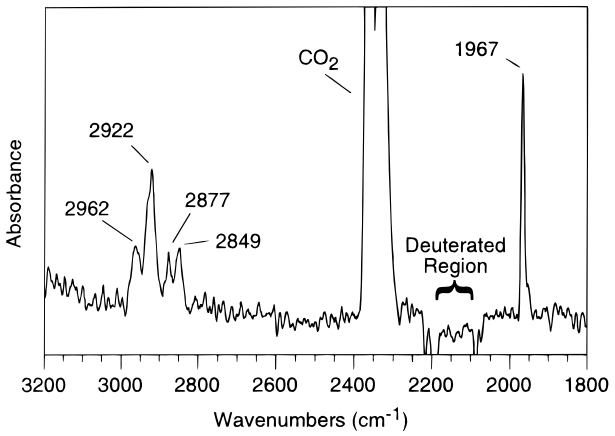

Figure 6. Grazing angle FT-IR spectra of a $\chi_{soln} = 0.75$ SAM/Ru(TMP)(CO). The stretching frequency of SAM/Ru(TMP)(CO), 1967 cm^{-1} (ν_{CO}), was shifted from the Ru(TMP)(CO) methylene chloride solution value of 1942 cm^{-1}. The negative peaks around 2150 cm^{-1} are due to the deuterated hexadecyl mercaptan SAM used as a background spectrum.

displayed two reversible redox waves. SAM/Ru(TMP)(CO) did not display reversible redox chemistry, which is also true of Ru(TMP)(CO)(L).

Grazing Angle FT-IR. The C−N stretch (ν_{CN}) of the acetonitrile axial ligands remaining after binding of $Ru(OEP)(CH_3CN)_2$, $Ru(OETAP)(CH_3CN)_2$, and $Os(OEP)(CH_3CN)_2$ to imidazole-terminated SAMs were too weak to be seen by p-polarized, grazing angle FT-IR. However, the C−O stretch (ν_{CO}) of the SAM/Ru(TMP)(CO) was clearly visible as a single, sharp peak at 1967 cm^{-1} (Figure 6), significantly shifted from that observed for this complex in methylene chloride solution (1942 cm^{-1}).

Scanning Tunneling Microscopy (STM). Ru(TMP)(CO) was adsorbed onto a SAM with low surface imidazole coverage ($\chi_{soln} = 0.25$) and imaged by constant current STM. Images were obtained in air for both the metalated and nonmetalated surfaces (Figure 7). High tunneling impedances of 0.6−33 GΩ were employed to minimize interactions between the tip and the surface.[33] Repeated scans of the same area reproducibly created the same image and showed no evidence of tip-induced damage to the substrate.

A 100 × 100 nm^2 image of the SAM with no adsorbed metalloporphyrin (Figure 7a) displayed characteristic "etch pits" formed during the chemisorption process as well as multiple steps in the underlying gold substrate.[33] A 100 × 100 nm^2 image of the SAM that had been treated with a Ru(TMP)(CO) solution, SAM/Ru(TMP)(CO), shows etch pits and gold steps similar to those of the nonmetalated SAM but also many disklike features (Figure 7b) consistent with metalloporphyrins. The disks also appear to be randomly spaced, suggesting that the imid-SH and C9-SH mercaptan components of this SAM are not highly phase separated.[34] A high-resolution image of a cluster of the disks, each approximately 2 nm in diameter, is shown on a 10 × 10 nm^2 scale in Figure 7c. Figure 8 shows a cross sectional plot through the middle of the central disk of Figure 7c taken along the horizontal scan direction. This cross section represents the height of the tip above the surface. A similar analysis of each disk in Figure 7c afforded an average height of 0.15 ± 0.04 nm and a width of 2.28 ± 0.05 nm. Using the X-ray structure of $Ru(TMP)(THF)(N_2)$ for comparison,[35]

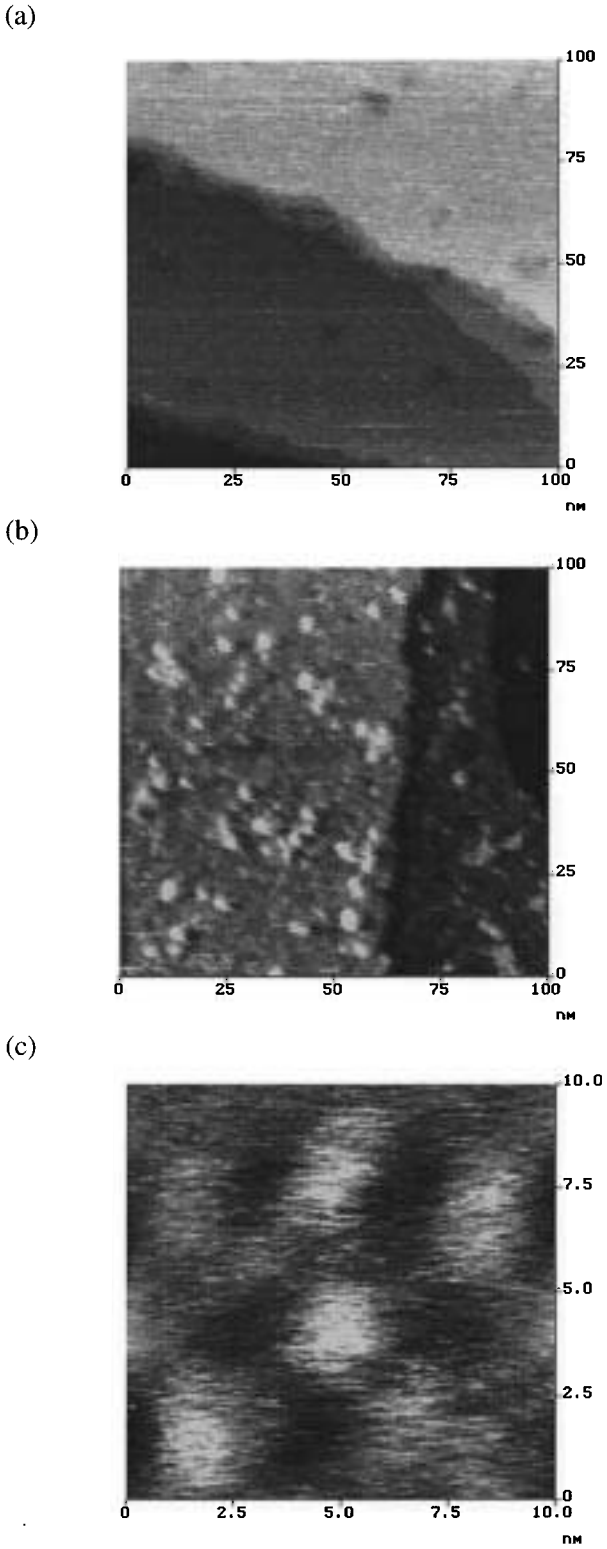

Figure 7. Scanning tunneling microscopy image of (a) a 100 × 100 nm^2 region (z scale = 3 nm, 30.52 pA, 1 V) of a $\chi_{soln} = 0.25$ SAM; (b) a 100 × 100 nm^2 image (z scale = 1.5 nm, 500 pA, 400 mV) of a $\chi_{soln} = 0.25$ SAM/Ru(TMP)(CO); and (c) a 10 × 10 nm^2 image (z scale = 0.6 nm, 500 pA, 300 mV) of a $\chi_{soln} = 0.25$ SAM/Ru(TMP)(CO). All images were obtained in height mode (constant current) and displayed in height-mapped gray scale with white corresponding to the highest and black the lowest features.

(33) (a) Widrig, C. A.; Alves, C. A.; Porter, M. D. *J. Am. Chem. Soc.* **1991**, *113*, 2805−2810. (b) Haussling, L.; Michel, B.; Ringsdorf, H.; Rohrer, H. *Angew. Chem., Int. Ed. Engl.* **1991**, *30*, 569−572. (c) Schonenberger, C.; Sondag-Huethorst, J. A. M.; Jorritsma, J.; Fokkink, L. G. J. *Langmuir* **1994**, *10*, 611−614. (d) Poirier, G. E.; Tarlov, M. J.; Rushmeier, H. E. *Langmuir* **1994**, *10*, 3383−3386.

(34) Folkers, J. P.; Laibinis, P. E.; Whitesides, G. M.; Deutch, J. *J. Phys. Chem.* **1994**, *98*, 563−571.

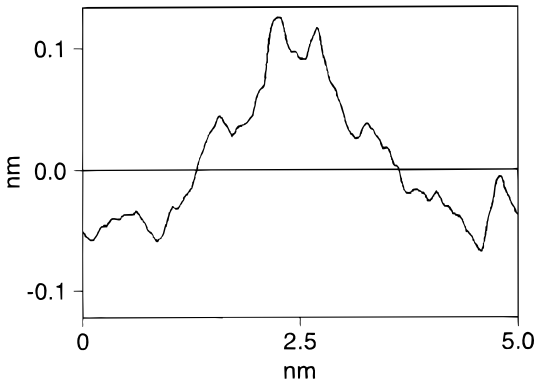

Figure 8. Cross sectional plot representing the tip height across the center of one of the features assigned to the metalloporphyrin of Figure 7c.

these dimensions are consistent with a metalloporphyrin bound by one axial site with its ring parallel to the SAM surface and the remaining axial site exposed and normal to the surface. A closer look at Figure 8 reveals that two cross sectional features were displayed by each disk: a set of inner peaks spaced 0.49 ± 0.07 nm apart and a set of outer peaks spaced 1.69 ± 0.04 nm apart. These peaks represent regions of high electron conductivity. The distance between the two inner peaks corresponds to the diameter of the inner porphyrin ring. The distance between the two outer peaks corresponds closely to the distance between opposite mesityl rings.

II. Axially Ligated, Bridged Metalloporphyrin Multilayers. Approach. The efficiency and generality of axial ligation of metalloporphyrins to imidazole-terminated SAMs suggest that these systems might serve as foundations for the construction of defined metalloporphyrin multilayer structures. The specific approach is outlined using bis-dinitrogen *meso*-tetramesitylporphyrinatoruthenium(II), Ru(TMP)$(N_2)_2$, and the bidentate ligand pyrazine (pyz) in Figure 9. Here, ligation of Ru(TMP)$(N_2)_2$ to the SAM (A) affords SAM/Ru(TMP)(N_2), which still bears a second labile axial ligand. Replacement of this ligand with pyrazine (B) results in SAM/Ru(TMP)/pyz, which presents a new axial ligand for a metalloporphyrin at the surface. Reaction of this assembly with Ru(TMP)$(N_2)_2$ (C) generates the bridged bilayer SAM/Ru(TMP)/pyz/Ru(TMP)(N_2), which can be elaborated to higher order multilayers through iteration of steps B and C, or capped with strongly binding axial ligands such as carbon monoxide (D). Use of the same metalloporphyrin in each cycle leads to the formation of single component stacked multilayers, while use of different metalloporphyrins provides mixed multilayer stacks. We have prepared examples of both single component and mixed multilayer metalloporphyrin stacks by this method. These materials have been characterized by transmission visible spectroscopy,[25] optical ellipsometry, XPS, advancing water contact angle goniometry, and grazing angle FT-IR.

Ru(TMP) Multilayers. Samples of SAM/Ru(TMP)(N_2) were prepared by immersing a $\chi_{soln} = 0.50$ mixed monolayer in a 1 mM solution of Ru(TMP)$(N_2)_2$ in benzene under an atmosphere of dinitrogen. The following capped stacks were assembled according to the scheme outlined in Figure 9: SAM/Ru(TMP)(CO), SAM/[Ru(TMP)/pyz/]$_n$Ru(TMP)(CO), $n = 1$, 2, 3, and 4. Replacement of dinitrogen axial ligands with pyrazine was effected by placing the surfaces in a methylene chloride solution of 1 mM pyrazine. Additional layers of

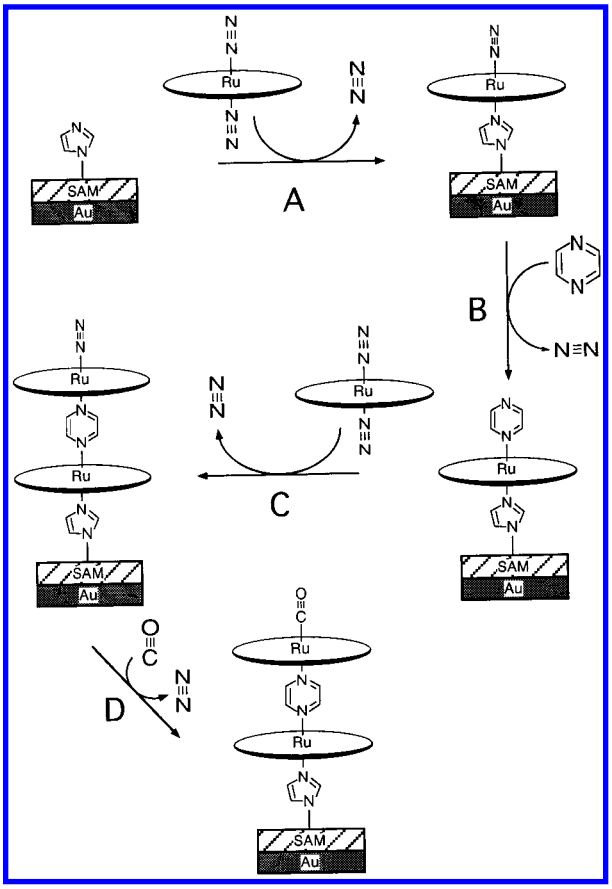

Figure 9. Deposition procedure and proposed mode of attachment of the Ru(TMP) double layer, capped with carbon monoxide, to a mixed SAM ($\chi_{soln} = 0.50$).

Table 2. Number of Porphyrin Layers, Ellipsometric Thicknesses for the SAM/Ru(TMP)[(pyz)Ru(TMP)]$_n$(CO) Series ($n = 0$, 1, 2, 3, 4) Compared with a $\chi_{soln} = 0.50$ SAM

	porphyrin thickness	
surface	layers	Å
$\chi_{soln} = 0.5$ SAM	0	14
SAM/Ru(TMP)(CO)	1	24
SAM/[Ru(TMP)(pyz)]$_1$Ru(TMP)(CO)	2	34
SAM/[Ru(TMP)(pyz)]$_2$Ru(TMP)(CO)	3	43
SAM/[Ru(TMP)(pyz)]$_3$Ru(TMP)(CO)	4	48
SAM/[Ru(TMP)(pyz)]$_4$Ru(TMP)(CO)	5	55

Ru(TMP)(N_2) were added by immersing pyrazine-terminated assemblies in a benzene solution of 1 mM Ru(TMP)$(N_2)_2$. Capping was carried out by placing the resulting surface under a CO atmosphere. After each step, the surfaces were thoroughly rinsed to remove excess ligand or metalloporphyrin.

Table 2 presents thicknesses as determined by ellipsometry data for the series of pyrazine-bridged Ru(TMP) multilayers. Increases in apparent film thickness of 5−10 Å were observed after each cycle, consistent with the incremental addition of pyrazine/Ru(TMP) units. XPS provided corroborating evidence for multilayer formation. The ratios of C(1s) and Ru(3d) peak intensities to Au(4f) peak intensities increased in step with the number of added metalloporphyrin layers.

Mixed Metalloporphyrin Bilayers. To explore the versatility of the general multilayer synthetic scheme, two bilayers containing Ru(TMP) and a second, different metalloporphyrin were prepared and compared to SAM/Ru(TMP)/pyz/Ru(TMP)-(CO). SAM/Ru(TMP)/pyz/Ru(TPFPP)(CO) was formed by addition of (*meso*-tetrakis(pentafluorophenyl)porphyrinato)-

(35) Camenzind, M. J.; James, B. R.; Dolphin, D.; Sparapany, J. W.; Ibers, J. A. *Inorg. Chem.* **1988**, *27*, 3054−3057.

Table 3. Ellipsometric Thicknesses, ν_{CO} Stretching Frequencies, and Advancing Water Contact Angles for the Metalloporphyrin Double Layers and the Corresponding CO-Capped Metalloporphyrin Building Blocks on $\chi_{soln} = 0.50$) SAM

surface	thickness (Å)	ν_{CO} (cm^{-1})	$\theta_a(H_2O)$
SAM	14		88.5
SAM/Ru(TMP)(CO)	24	1967	88
SAM/Ru(TMP)(pyz)Ru(TMP)(CO)	35	1974	88
SAM/Os(OEP)(CO)	25	1917	88
SAM/Ru(TMP)(pyz)Os(OEP)(CO)	36	1978	81
SAM/Ru(TPFPP)(CO)	27	1998	97
SAM/Ru(TMP)(pyz)Ru(TPFPP)(CO)	30	2002	83

ruthenium(II) (Ru(TPFPP)) to SAM/Ru(TMP)/pyz, followed by capping with CO. SAM/Ru(TMP)/pyz/Os(OEP)(CO) was formed by addition of five-coordinate Os(OEP)(CO) to SAM/Ru(TMP)/pyz.

Table 3 presents ellipsometric thicknesses, CO stretching frequencies, and advancing water contact angles for both the single component and mixed metalloporphyrin bilayers and monolayers bearing the corresponding metalloporphyrin building blocks. SAM/Ru(TPFPP)(CO) was prepared by axial ligation of Ru(TPFPP) to a $\chi_{soln} = 0.50$ SAM and CO capping. The differences in observed thicknesses for SAM/Ru(TMP)/pyz/Os(OEP)(CO) versus SAM/Os(OEP)(CO) and SAM/Ru(TMP)/pyz/Ru(TMP)(CO) versus SAM/Ru(TMP)(CO) were identical (11 Å). The presence of Ru(TPFPP)(CO) on the surface was clearly indicated by the ν_{CO} observed at 2002 cm^{-1} for this system relative to 1998 cm^{-1} for SAM/Ru(TPFPP)(CO). In addition, a large F(1s) photoelectron peak was observed in the XPS of this surface along with splitting of the C(1s) peak due to the electron-withdrawing effect of the fluorine substituents attached to carbon. In each of the bilayer structures, CO stretching frequencies were found at higher frequencies than those in the corresponding monolayers. This shift was quite dramatic with SAM/Ru(TMP)/pyz/Os(OEP)(CO) versus SAM/Os(OEP)(CO), where ν_{CO} values were 1978 and 1917 cm^{-1}, respectively. The shifts to higher frequency are consistent with CO being bound opposite to pyrazine, which is a stronger π-acid than imidazole.

We have also prepared the mixed bilayer SAM/Ru(TPFPP)/pyz/Ru(TMP)(CO) and the alternating trilayer SAM/Ru(TMP)/pyz/Ru(OEP)/pyz/Ru(TMP)(CO).[36] In synthesizing the trilayer, the bis(pyrazine) complex Ru(OEP)$(pyz)_2$ was adsorbed directly onto SAM/Ru(TMP)(N_2), and Ru(TMP)(CO) was added to cap the SAM/Ru(TMP)/pyz/Ru(OEP)/pyz assembly. Thus, we were able to bypass several steps of the general multilayer synthetic scheme by using Ru(OEP)$(pyz)_2$ as a bidentate ligand with a metalloporphyrin core.

Discussion

Site Specific Binding. An important conclusion that can be drawn from the XPS, electrochemistry, ellipsometry, and goniometry data is that Ru(OEP)(CH_3CN) binds specifically to the imidazole terminus of the 1-(10-mercaptodecyl)imidazole and not to the methyl terminus of the unsubstituted alkanethiol. No evidence for Ru(T-*p*-ClPP)(CH_3CN) deposition on the full C9-SH SAM ($\chi_{SAM} = 0$) was found. The amount of bound Ru(OEP)(CH_3CN) was directly related to the quantity of 1-(10-mercaptodecyl)imidazole in the SAM, reaching a maximum with the full 1-(10-mercaptodecyl)imidazole SAM ($\chi_{SAM} = 1$) surface as shown by ellipsometry but not by advancing water contact angles. Goniometry indicates that a uniform surface was achieved by metalloporphyrin adsorption to a $\chi_{soln} = 0.50$ surface, suggesting that, at higher values of χ_{SAM}, some of the bound metalloporphyrins were physisorbed. It may be that specifically bound metalloporphyrins serve as nucleation sites for the formation of physisorbed multilayer structures. The value of χ_{SAM} calculated to give complete coverage of the SAM by Ru(OEP)(CH_3CN) ($\chi_{SAM} = 0.11$ if the imid-SH adsorbates are regularly distributed in the SAM) is expected to increase if the imid-SH adsorbates are *randomly* distributed in the SAM. Our results suggest that SAMs with $\chi_{soln} < 0.50$ will afford metalloporphyrins bound in the most uniform manner.

Axial Substitution. Four results provide evidence that metalloporphyrins are axially ligated to the imidazole groups presented at the surface of a SAM. First, the location, strength, and sharpness of the ν_{CO} stretch in the grazing angle FT-IR spectrum of SAM/Ru(TMP)(CO) provide important information about the orientation and environment of the CO at the surface. The change in the carbonyl IR stretching frequency from the free Ru(TMP)(CO) to the surface-bound Ru(TMP)(CO) is 25 cm^{-1}. This indicates a distinctly different ruthenium carbonyl bonding environment for the two species. Furthermore, the direction of the change implies that the ruthenium carbonyl bond is stronger in the free Ru(TMP)(CO) species than in the surface-bound species as expected from the trans influence of a ruthenium imidazole bond.[37] p-Polarized light interacts with dipoles that have a component perpendicular to the surface.[38] The strength of the CO signal compared to the methylene stretches indicates that the CO dipole has a large component normal to the surface. In addition, the surface CO stretch was very sharp, suggesting a single CO containing species. These IR data are consistent with a SAM-bound metalloporphyrin having the porphyrin ring oriented parallel and the CO ligand normal to the surface, as depicted in Figure 1. Second, protonation of the imidazole of the SAM completely inhibited its reaction with Ru(OEP)$(CH_3CN)_2$. Third, attaching strongly bound axial ligands to the metalloporphyrin also prevented adsorption to the SAM. Fourth, STM analysis of Ru(TMP)(CO) adsorbed on SAMs gave images consistent with a model in which metalloporphyrins lie flat on the SAM. At the low surface imidazole concentration employed in these experiments, the metalloporphyrins appear as randomly spaced disks on the SAM surface. At high resolution, the sizes of the disks are in agreement with crystal structure analysis of Ru(TMP)(CO).

Generality and Advantages. Several metalloporphyrins were found to bind to mixed imidazole/methyl-terminated SAMs under the same conditions employed in the SAM/Ru(OEP)(CH_3CN) study. Variation of the porphyrin ring (from OEP to TMP, OETAP, and TPFPP) and the metal (from Ru to Os) did not significantly hinder the formation of surface-bound complexes. Our results indicate that this method can be used for the general binding of any metalloporphyrin that displays high affinity for the ligand presented by a self-assembled monolayer. Indeed, this method could be generalized to many other situations where metal ions or complexes exhibit significant affinity for ligands which can be presented at the surface of a SAM. Due to the site specific binding of the metalloporphyrin and the sensitivity of the various surface analytical techniques available, this method requires only small amounts of material and no synthetic modification of the metalloporphyrin.

(36) Ennis, M. S., Ph.D. Thesis, Stanford University, Stanford, CA, 1995.

(37) Collman, J. P.; Hegedus, L. S.; Norton, J. R.; Finke, R. G.; *Principles and Applications of Organotransition Metal Chemistry*; University Science Books: Mill Valley, CA 1987.

(38) (a) Porter, M. D. *Anal. Chem.* **1988**, *60*, 1143A−1155A. (b) Pearce, H. A.; Sheppard, N. *Surf. Sci.* **1976**, *59*, 205−217.

Single Component and Mixed Multilayer Metalloporphyrin Stacks. By taking advantage of the high affinity of metalloporphyrins for the bidentate ligand pyrazine, we have developed a simple and flexible route to electrode-bound metalloporphyrin multilayers in which a gold-supported SAM/metalloporphyrin serves as the base. The pyrazine-bridged multilayers prepared are immobilized analogues of the highly conductive, soluble metalloporphyrin polymers reported by Collman et al.[39] The controlled, iterative, and general nature of the method defines it as a form of solid-phase synthesis and suggests that it could be exploited in a combinatorial fashion[12g] for the preparation and screening of new metalloporphyrin-based materials.[12]

Acknowledgment. This work was supported by the National Science Foundation and the Arnold and Mabel Beckman Foundation. We also thank the Center for Materials Research at Stanford University for use of the STM and the XPS made possible through funds from the NSF-MRSEC program. We acknowledge the Mass Spectrometry Facility of the University of California at San Francisco, supported by NIH Division of Research Resources Grant RR01614 and by NSF Grant DIR8700766. We also thank Dr. H. T. Fish and Dr. J. Kendall for providing the H_2TMP and H_2OETAP ligands, respectively.

(39) Collman, J. P.; McDevitt, J. T.; Leidner, C. R.; Yee, G. T.; Torrance, J. B.; Little, W. A. *J. Am. Chem. Soc.* **1987**, *109*, 4606−4614.

Supporting Information Available: Grazing angle FTIR and transmission visible spectra of SAM/metalloporphyrins complexes discussed in this paper as well as the relevant experimental detail and discussion. XPS spectra of Ru(Tp-ClPP)(CO)(CH_3CN) in a KBr matrix and on an imidazole surface are presented. Additionally, a proposed hexagonal packing arrangement of the porphyrins on an ideal SAM surface is shown, along with geometric arguments for calculating the "ideal" effective area of porphyrins arranged in this way. (12 pages, print/pdf). See any current masthead page for ordering information and Web access instructions.

JA973528L